Science of the Total Environment xxx (xxxx) xxx

Contents lists available at ScienceDirect

Science of the Total Environment

journal homepage: www.elsevier.com/locate/scitotenv

Impact of different roofing mitigation strategies on near-surface temperature and energy consumption over the Chicago metropolitan area during a heatwave event

Haochen Tan [a,*], Rao Kotamarthi [a], Jiali Wang [a], Yun Qian [b], T.C. Chakraborty [b]

[a] Environmental Science Division (EVS), Argonne National Laboratory, Lemont, IL, United States
[b] Atmospheric Sciences and Global Change Division, Pacific Northwest National Laboratory, Richland, WA, United States

HIGHLIGHTS

- The use of solar photovoltaic panels has surged in the cities recently.
- Urban atmosphere model compares scenarios for installing cool roofs, green roofs, and solar panel roofs during heatwave event.
- Best cooling energy saving when solar panel roofs are applied.

GRAPHICAL ABSTRACT

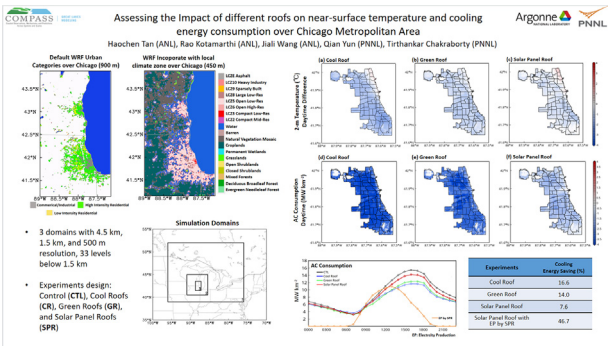

ARTICLE INFO

Editor: Shuqing Zhao

Keywords:
Heatwave
Rooftops
Cooling energy demand
Urban climate modeling

ABSTRACT

This study examined the impact of cool roofs, green roofs, and solar panel roofs on near-surface temperature and cooling energy demand through regional modeling in the Chicago metropolitan area (CMA). The new parameterization of green roofs and solar panel roofs based on model physics has recently been developed, updated, and coupled to a multilayer building energy model that is fully integrated with the Weather Research and Forecasting model. We evaluate the model performance against with observation measurements to show that our model is capable of being a suited tool to simulate the heatwave event. Next, we examine the impact by characterizing the near-surface air temperature and its diurnal cycle from experiments with and without the different rooftops. We also estimate the impact of the rooftop on the urban island intensity (UHII), surface heat flux, and the boundary layer. Finally, we measure the impact of the different rooftops on citywide air-conditioning consumption. Results show that the deployment of the cool roof can reduce the near-surface temperature most over urban areas, followed by green roof and solar panel roof. The cool roof experiment was the only one where the near-surface temperature trended down as the urban fraction increased, indicating the cool roof is the most effective mitigation strategy among these three rooftop options. For cooling energy consumption, it can be reduced by 16.6 %, 14.0 %, and 7.6 %, when cool roofs, green roofs, and solar panel roofs are deployed, respectively. Although solar panel roofs show the smallest reduction in energy consumption, if we assume that all electricity production can be applied to cooling demand, we can expect almost a savings of almost half (46.7 %) on cooling energy demand.

* Corresponding author at: Argonne National Laboratory, 9700 S. Cass Ave., Lemont, IL 60439, United States.
E-mail address: htan@anl.gov (H. Tan).

http://dx.doi.org/10.1016/j.scitotenv.2022.160508
Received 9 September 2022; Received in revised form 31 October 2022; Accepted 22 November 2022
Available online xxxx
0048-9697/Published by Elsevier B.V. This is an open access article under the CC BY-NC-ND license (http://creativecommons.org/licenses/by-nc-nd/4.0/).

Please cite this article as: H. Tan, R. Kotamarthi, J. Wang, et al., Impact of different roofing mitigation strategies on near-surface temperature an..., Science of the Total Environment, http://dx.doi.org/10.1016/j.scitotenv.2022.160508

1. Introduction

Deployment of cool or green roofing technology on a broad scale can mitigate urban heat and reduce energy consumption and has been proposed widely for these purposes (Akbari et al., 2009; Salamanca et al., 2012a; Li et al., 2014; Santamouris, 2014; Georgescu et al., 2014; Zhang et al., 2017; Tan et al., 2019; Zhang et al., 2019; Zonato et al., 2021). Both cool and green roofs can reduce heat storage in buildings (thus cooling them), but their mechanisms differ. Because cool roofs increase albedo (or surface reflectivity), they absorb less incoming shortwave radiation than conventional roofs, leading less heat into the urban canopy and eventually reducing surface temperature through the mixing of air. Consequently, cool roofs limit the transmission of heat into urban interiors and the broader environment, reducing air-conditioning consumption and near-surface temperature, respectively. Green roofs, on the other hand, can convert available energy more efficiently than conventional roofs into latent heat flux through vegetation by increasing evapotranspiration on the rooftop and lowering sensible heat flux transfer into the urban surface layer.

The immediate advantages of large-scale implementation of cool and green roofs in urban areas have been demonstrated at a building or neighborhood scale (Wong and Chen, 2005; Jaffal et al., 2012; Sun et al., 2013, 2014; Kong et al., 2016). However, because of the significant influence of surface heterogeneity on the local microclimate, the effects of mitigation approaches applied at these scales may not easily translate to city-scale benefits (Bou-Zeid et al., 2004, 2007; Li et al., 2014). Furthermore, upscaling from the buildings to the city may not capture the impacts of individual building rooftops on outside urban air temperatures, the exchanges of air temperature/moisture, and surface energy balances (Li et al., 2014).

Numerical weather prediction (NWP) models have been used frequently to quantify the impacts of green/cool roofs at the city scale (Synnefa et al., 2008; Millstein and Menon, 2011; Georgescu et al., 2013; Li et al., 2014; Li and Norford, 2016; Sun et al., 2016; Zhang et al., 2017; Yang et al., 2016; Morini et al., 2017; Zonato et al., 2021). Millstein and Menon (2011) showed that nationwide cool roof deployment over the United States would lower summertime air temperature by 0.11–0.53 °C based on 12 simulated summer periods using a model with a 25-km grid spacing. Georgescu et al. (2013) demonstrated that the regional warming over Arizona caused by urbanization could be moderated by 50 % by using cool roofs. For the Baltimore-Washington region, it has been shown that surface air temperature could be lowered by 3.5 °C by green roofs and 2 °C by cool roofs (Li et al., 2014). Over the Yangtze River Delta in China, researchers found that green and cool roofs could lower the daily mean surface air temperature by 1 °C and 3.8 °C, respectively (Zhang et al., 2017).

However, cool roofs and green roofs are not the only roofing options that can mitigate heat and reduce electricity consumption. Recently, the use of solar photovoltaic panels has surged in the cities. Dominguez et al. (2011) showed that in San Diego, California, solar photovoltaic panels that partially cover building rooftops can reduce not only greenhouse gas emissions but also the annual cooling load. Salamanca et al. (2016) found that solar photovoltaic panels could lower the 2-m temperature over Phoenix and Tucson, Arizona. Ma et al. (2017) found that solar photovoltaic panels might reduce summer maximum temperatures in Sydney. In a study that corroborates these findings, Taha (2013) demonstrated that a vast solar panel deployment across the Los Angeles area has a cooling effect of up to 0.2 °C. Conversely, the study by Zonato et al. (2021) exhibits this differently: solar panels can induce a temperature increase during the daytime due to less efficient heat release and more sensible heat flux together from solar panels and the roof.

Earlier studies have presented comprehensive effects of various roofing technologies, including cool roofs, green roofs, and solar panel roofs, on air temperature. However, some of these studies focus only on the building or neighborhood scale. Also, among studies that use NWP models at the urban scale, some employ only single-layer urban parameterization instead of multi-layer urban parameterization, even though the multi-layer option can simulate the three-dimensional urban structure. To fully examine the impact of different roofing mitigation strategies on urban climate and energy demand, we use a high-resolution regional scale modeling system (500 m grid spacing) fully coupled with a building energy model. The spatial resolution of the World Urban Database and Access Portal Tools (WUDAPT, Ching et al., 2018) is 100 m, which it has rendered to NWP model resolution (500 m) in this study. Our goal is to evaluate and compare the regional impacts of the extensive deployment of cool roofs, green roofs, and solar photovoltaic panel roofs on near-surface temperature and air-conditioning (AC) consumption in the Chicago region. To the best of our knowledge, little research has been done to evaluate these three roof mitigation strategies collectively over Chicago.

In this paper, we introduce the mechanism of the three roof technologies and thus assess the impacts of the cool roof, green roof, and solar panel roofs technologies on near-surface temperature and energy consumption from air-conditioning by using the building model used Building Effect Parameterization coupled with the Building Energy Model (BEP + BEM, Martilli et al., 2002; Salamanca and Martilli, 2010) in Weather Research and Forecasting (WRF) regional climate model (version 4.3.1; Skamarock et al., 2021). We first evaluate the model performance against with observation measurements to show that our model is capable of being a suited tool to simulate extreme weather conditions. Next, we examine the impact by characterizing the near-surface air temperature and its diurnal cycle from experiments with and without the rooftop. We also estimate the impact of the rooftop on the urban island intensity (UHII) and surface heat flux, and finally, we measure the impact of the different rooftops on citywide air-conditioning consumption. We characterize these factors for different roofs in the Chicago metropolitan area (CMA). The 1995 heatwave in the CMA resulted in the highest recorded mortality rates during a heat wave in North America (Livezey and Tinker, 1996). In recent decades, an increasing warming trend has been documented in the region, resulting in increased human health hazards and energy consumption (Chen et al., 2022). The regional climate of CMA is moderated by its adjacency to Lake Michigan and the natural lake breeze occasionally mitigates UHI (Davies et al., 2007; Harris and Kotamarthi, 2005). However, the lake breeze is not an effective solution most days and for all the CMA and it is important to understand whether the broad deployment of rooftop mitigation strategies over CMA would be effective for UHI mitigation in the face of the increasing warming trends. Methodology and simulation designs are outlined in Section 2. The results are in Section 3, and the summary and conclusions are in Section 4.

2. Methodology

2.1. Modeling system and land use

We ran a regional climate model combined with a multi-layer building system over CMA. The model for the climate was the non-hydrostatic and fully compressible Weather Research and Forecasting (WRF) regional climate model (version 4.3.1; Skamarock et al., 2021). The building model used Building Effect Parameterization coupled with the Building Energy Model (BEP + BEM, Martilli et al., 2002; Salamanca and Martilli, 2010) was used to simulate the diurnal variation of near-surface temperature and cooling energy consumption over the city. The BEP model was developed and validated offline by Salamanca et al. (2010) and implemented in Salamanca et al. (2010). The BEP + BEM system calculates the surface momentum, heat exchanges, humidity, and turbulent kinetic energy fluxes to the atmospheric dynamics governing equations under atmospheric conditions at the WRF bottom level. Hence, the coupling of the BEP + BEM system with WRF is accomplished. Compared to Single-Layer Urban Canopy Model (SLUCM, Kusaka et al., 2001), the BEP + BEM model takes into account 1) the three-dimensional urban structure in a model grid using multiple layers and the origins and sinks of momentum and heat in the vertical layers within the urban canopy layer, 2) the impact of horizontal and vertical surfaces (such as roads and walls) on the momentum, turbulent kinetic energy, and potential temperature, 3) the shading, reflection and blocking effect of horizontal and vertical surfaces on net

solar radiation within the urban canopy layer, 4) exchange of heat between building walls, rooftops, and floors, 5) heat discharged by people and domestic electrical appliance and 6) air-conditioning cooling, heating, and ventilation (Salamanca and Martilli, 2010; Ribeiro et al., 2020; Ricard et al., 2021).

Quantifying the physical processes within an urban region requires an accurate description of advanced urban geometry. Thus, for this study, an integrated spatial model of local climate zones (LCZ) was created, a concept defined and developed by Stewart and Oke (2012). The new version of WRF-Urban and BEP + BEM urban multi-layer parameterization can integrate 11 urban classifications from WUDAPT. This method has already been implemented in many studies (Brousse et al., 2016; Zonato et al., 2020; Hammerberg et al., 2018; McRae et al., 2020; Patel et al., 2020). The LCZ is the level 0 product produced by WUDAPT and incorporates different land use categories with comparable long-term meteorological features. Foley (2015) created the LCZ database for the CMA region, which categorizes areas into 11 classifications instead of the traditional three urban categories. Another update in this WRF-Urban is that a new buildings drag coefficient that induced by buildings for mean wind speed and turbulent kinetic energy is applied and its improvement to the model have shown by Gutiérrez et al. (2015) and Santiago and Martilli (2010).

2.2. Numerical modeling of cool roofs, green roofs, and solar panel roofs

Fig. 1 shows the basic concept of a grid cell with built impervious fractions and different types of roofs for urban buildings. The impervious part of the urban canopy includes buildings, roads, and pavements. The surface energy balance for the conventional rooftop is presented by

$$SW_{Net} + LW_{Net} + AH = LH + SH + G \quad (1)$$

where SW_{Net} is the net shortwave radiation at the surface, LW_{Net} is the net longwave radiation at the surface, AH is the anthropogenic heat flux, LH and SH are the latent and sensible heat flux, and G is the ground heat flux. For BEP + BEM in WRF, the anthropogenic heat flux represented is from air-conditioning, heat exchanges between the building interior and exterior air, and the heat released by equipment and people within the buildings. This is a limitation of BEP + BEM: BEP + BEM treats the factors above as the only anthropogenic heat sources, where it does not include anthropogenic heat from traffic or industry. For a traditional roof, all net radiation is transferred into sensible heat flux and heat flowing into the building, raising the skin temperature and near-surface temperature. Cool roofs can lower the net radiation at the roof by reflecting the shortwave radiation from the reflective roofing material.

The green roof parameterization has been established according to de Munck et al. (2013) and it was recently updated by Zonato et al. (2021). The parameterization for green roofs computes energy and water supply, estimates net radiation, water contribution from precipitation and irrigation, vegetation evapotranspiration, heat transmission, and energy and moisture distribution through the soil. The green roof scheme in this WRF version incorporates ten layers including five levels of organic matter substrate where the plant grows, one layer of drainage, and four levels of the insulation layer, with a total of ~0.3 m. A complete description of hydrology and thermodynamics for green roofs can be found in Zonato et al. (2021).

The parameterization of solar photovoltaic panel roofs in the WRF model was previously developed by Masson et al. (2014) and the new parameterization has been developed and tested by the developers in the latest version of WRF model (Zonato et al., 2021). The solar panels in this parameterization are assumed to be parallel and unattached from the roof so that not only the profiles of individual buildings can remain simple but also the shading effect of solar panels decreases the surface temperature of the roof from the shading effect The temperature over solar panels roof and its associated heat fluxes are determined by the derivative equation below with all terms in W m^{-2}:

$$C_{module}\frac{\partial T_{PV}}{\partial t} = (1-\alpha_{PV})SW^{\downarrow}_{sky} + \varepsilon^{U}_{PV}LW^{\downarrow}_{sky} - LW^{\uparrow}_{PV} + LW^{\uparrow\downarrow}_{roof-PV} - E_{PV} - SH^{\uparrow} - SH^{\downarrow} + (1-VF) \times \left[(1-\alpha_{PV})SW_{DIFF} + LW^{\downarrow}_{sky}\right] \quad (2)$$

where C_{module} is the equivalent heat capacity per unit area, α is albedo. The terms on the right-hand side are net shortwave radiation gained by the upward surface of the solar panel; the incoming longwave radiation at the upper surface of the solar panel where the ε^{U}_{PV} is the emissivity of the glass face; upward longwave radiation emitted by solar panel; longwave radiation exchanged between the monocrystalline silicon downward face of the solar panel and the upward of the roof; energy production by solar panel; upward sensible heat flux from the solar panel; downward sensible heat flux from solar panel; diffuse shortwave and longwave isotropic radiations reaching the downward solar panel surface where VF is the view factor between downward face of the solar panel and the roof. More explanation of this equation can be found in Zonato et al. (2021).

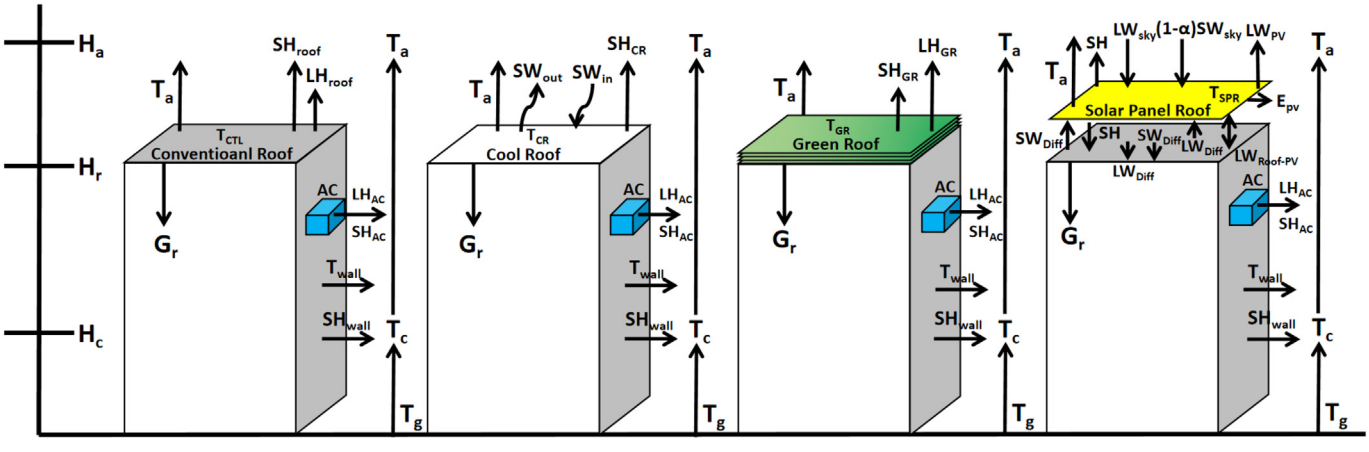

Fig. 1. Schematic description of urban grid cell applied in WRF for (left to right) conventional roof, cool roof, green roof, and solar panel roof modeling. H_a is the height of first level in the atmospheric model, H_r is the height of the building rooftop, and H_c is the canopy height. SH and LH represent sensible and latent heat flux, respectively. T_a signifies the temperature at the beginning level of the atmospheric model. T_c is the temperature at canopy level. T_g is the surface temperature. T_{wall} is the temperature from the building wall. SW and LW are shortwave and longwave radiation, respectively, and G_r is the ground heat flux into the building. E_{pv} characterizes the electricity generated by solar panels. The blue box on the side on the building represents the AC unit. The length of each arrow does not represent the magnitude of each variable. The detailed description of parameterization is in Section 2.2.

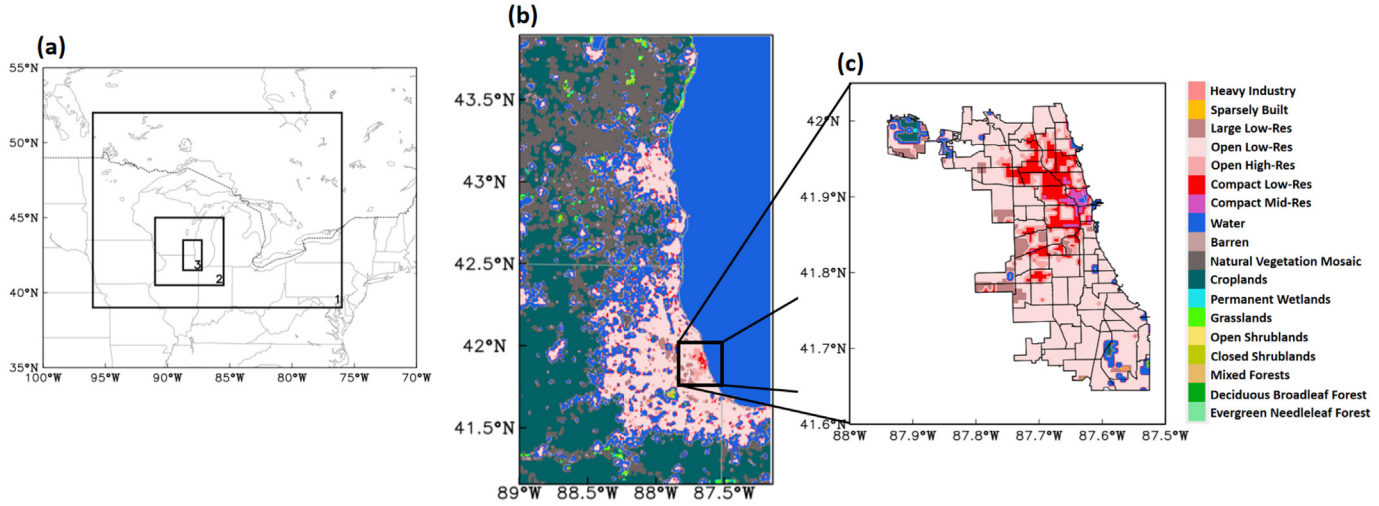

Fig. 2. (a) WRF domain configuration. The outer domain (1), the middle domain (2), and the inner domain (3) have a resolution of 4.5 km, 1.5 km, and 500 m, respectively. (b) Urban land-use categories (shading) after the incorporation of local climate zones (LCZs) from WUDAPT data over domain 3. (c) Same as in (b) but for Chicago Metropolitan Area. The domain in (c) is the area used the analysis.

The configuration of solar panel roof parameterization is defined as "PV_FRAC_ROOF" in the URBPARAM_LCZ.TBL to arrange the coverage fraction over buildings. Compared to the parameterization from Masson et al. (2014) and Salamanca et al. (2016), the temperature on solar panels roof in the new parameterization is solved numerically from the derivative equation instead of parameterizing the temperature through its dependence on shortwave solar radiation, contributed by all the associated components (Zonato et al., 2021). Other heat flux will be updated and proceeds to other urban sections after the solar panel roof temperature is computed. In our solar panel experiment, we assume the roofs are entirely covered with solar panels (i.e., the fraction of solar panel equal 1).

2.3. Model set-up and experiment design

This study targets CMA and its neighboring rural areas, centered on 41°52′54″N, 87°37′23″W. Three two-way nested domains were used with 406 × 313 grid points in domain 1, 280 × 382 in domain 2, and 292 × 583 in domain 3, with grid spacing of 4.5, 1.5, and 0.5 km in WRF 4.3.1, respectively (Fig. 2a). The outermost parent domain includes the entire Great Lakes, and the innermost domain encloses CMA. The LCZ classifications are integrated in the WRF model by updating the surface parameters for every grid in the innermost domain. As such, the initial MODIS land use categories have been added an extra 11 urban categories to allow WRF to use the specialized categories in the LCZ model we have chosen (Fig. 2b). The details including the workflow about how to ingest LCZ information into WRF can be found in Demuzere et al. (2020, 2022). Non-urban land covers are based on the Moderate Resolution Imaging Spectroradiometer (MODIS) 21-class product (Kumar et al., 2014). For the length of the simulation (6 days), the size of the outermost domain was sufficient to capture synoptic phenomena throughout the domain. We use the 51 eta levels for vertical grid-spacing as in Salamanca et al. (2012a,b): these range from surface to 100 hPa, with 38 levels located below 2 km and with the model top over about 20 km. The integration time step was 20 s for the outermost domain, and the simulation outputs were collected every 15 min for the innermost domain. The initial and boundary conditions were taken from the National Centers for Environmental Prediction Final Analysis data (NCEP-FNL, 1° × 1°, 6-hourly). In this study, we used the unified Noah land-surface model for the land-surface scheme (Chen and Dudhia, 2001; Ek et al., 2003), the Mellor-Yamada-Janjic scheme for the planetary boundary layer (Janjic, 2002), the WRF Single Moment 6 for microphysics (Hong and Lim, 2006), the Dudhia scheme for shortwave radiation (Dudhia, 1989), the Rapid Radiative Transfer Model for longwave radiation (Mlawer et al., 1997), and the Monin-Obukhov-Janjic approach (Janjic, 2002) for the surface-layer scheme. No cumulus parameterization was used.

Four experiments were conducted, all including the same 6-day, clear-sky period from August 21 (0000 LT) to August 27 (0000 LT), 2021, to estimate the regional effects of extensive deployment of different roofs on near-surface temperature and AC consumption. A heatwave event occurred on August 24, 2021, with the temperature reaching a high of 35 °C (95 °F) in the Chicago area. The control simulation (CTL, Table 1) was run using a roofs albedo of 0.2 as the baseline case, with no green roofs/solar panels. The cool roof simulation (CR, Table 1) emulated the impact of cool roofs by setting the urban roof albedo to 0.8. Similarly, the green roof simulation (GR, Table 1) addressed the impact of the green roofs by setting the green roof fraction to 1 for each urban roof. Finally, the solar panel roof experiment (SPR, Table 1) set each urban roof's solar panel fraction equal to 1. The albedo, conversion efficiency, and emissivity for solar panel roofs were set to 0.2, 0.19, and 0.90, respectively, which are standard numbers for the current solar panel equipment. Based on the study by Demuzere et al. (2020), we altered the default urban parameters used in the urban parameterization, namely, urban fraction, road and roof width, thermal properties, heat capacity, and emissivity. The values applied for these simulations are summarized in Table 2. The thermal properties of different roofs are demonstrated in Table 3, taken from Sun et al. (2013), Li et al. (2014), and Zonato et al. (2021). Table 4 summarized the urban parameters that were applied in this study. We excluded the coverage of cool roofs, green roofs, and solar panel roofs on three LCZ land use categories: Sparsely Built (LCZ 9), Heavy Industrial (LCZ 10), and Rock and Paved (LCZ E), as these three categories are not ideal for roof deployment.

2.4. Observational data

To evaluate the model performance for near-surface meteorologies, such as 2-m temperature and 10-m wind speed, we compared observations from six weather stations (Table 5) over CMA against the simulated values.

Table 1
Summary of experiments performed.

Experiment	Roof type
Control (CTL)	Conventional roof with albedo equal to 0.2
Cool roof (CR)	Roof with albedo equal to 0.8
Green roof (GR)	Green roof fraction equal to 1
Solar panel roof (SPR)	Solar panel roof fraction equal to 1

Table 2
Modified urban parameters that used in this study for 4 main urban categories (LCZ3, LCZ5, LCZ6, LCZ8), which also include the thermal properties for conventional roof on each category.

LCZ name and designation	LCZ 3	LCZ 5	LCZ 6	LCZ 8
Urban fraction (−)	0.9	0.7	0.65	0.85
Road and roof width (m)	5.7	33.3	12.4	32.5
Surface albedo of road/roof/wall (−)	0.2/0.2/0.15			
Thermal conductivity of road (J m^{-1} s^{-1} K^{-1})	1.00	1.25	1.00	1.25
Thermal conductivity of roof (J m^{-1} s^{-1} K^{-1})	1.25	1.45	1.25	1.25
Thermal conductivity of walls (J m^{-1} s^{-1} K^{-1})	0.69	0.62	0.60	0.80
Heat capacity of road (J m^{-3} K^{-1})	1.63e6	1.50e6	1.47e6	1.8e6
Heat capacity of roof (J m^{-3} K^{-1})	1.44e6	1.8e6	1.44e6	1.8e6
Heat capacity of walls (J m^{-3} K^{-1})	2.05e6	2.0e6	0.72e6	1.8e6
Emissivity of road (−)	0.95			
Emissivity of roof (−)	0.90			
Emissivity of walls (−)	0.90			

Table 3
Thermal properties of different roofs. For solar panel roof, the depth of the solar panel is 6.55 mm. The solar panel height away from the building's top surface is 80 cm. Detail can be found in Zonato et al. (2021).

	Cool roof	Green roof	Solar panel roof
Albedo (−)	0.8	0.25	0.2
Emissivity (−)	0.9	0.9	0.9
Heat capacity (MJ m^{-3} K^{-1})	2.0	1.9	5.72
Thermal conductivity (J m^{-1} s^{-1} K^{-1})	1.0	1.1	1.0
Roof depth (cm)	20	30	0.0655 + 80

Table 4
Urban canopy parameter data associated with LCZ types in WRF.

LCZ	Urban fraction	Vegetation fraction	Average building height (m)	Road width (m)
1. Compact highrise	1	0	35	15
2. Compact midrise	0.95	0.05	16.75	12.7
3. Compact lowrise	0.9	0.1	7.25	5.7
4. Open highres	0.65	0.35	33.5	37.5
5. Open midrise	0.7	0.3	19	33.3
6. Open lowrise	0.65	0.35	6.75	12.4
7. Lightweight lowrise	0.85	0.15	5	2.0
8. Large lowrise	0.85	0.15	8.25	32.5
9. Sparsely built	0.3	0.7	6.25	10.5
10. Heavy industry	0.55	0.45	11	28.5

Four of the stations are considered urban and two are rural. It is important to highlight that, even though the experiment has a high resolution (500 m for the innermost domain) compared to earlier research, more spatial variability should be expected in the observations compared to the model because a 500 m × 500 m grid cell can still include various land-use types; hence, misclassifications could exist between a grid cell's land-use type and a station's footprint (Sharma et al., 2016). Daytime is defined as 1100 to 1700 local standard time (LST) and nighttime as 0000 to 0600 LST.

2.5. Quantifying urban heat island intensity (UHII)

There are various methods to calculate the UHII (Liao et al., 2018; Li et al., 2019; Chen et al., 2022). Here we use the method of Li et al. (2019), where the relationship between temperature and the urban fraction (FRC_URB) is a linear equation given by

$$T = FRC\_URB \times UHII + T_{vegetation} \quad (3)$$

where the urban fraction becomes the independent variable. The slope of this equation is the UHII, and the intercept is the baseline temperature over a completely pervious surface, which in this region is primarily croplands. We exclude areas that have open water bodies in this calculation. The FRC_URB is acquired from MODIS and LCZ in WUDAPT; the value reflects the degree of urbanization and the portion of impervious areas.

2.6. Assessing heat index (HI)

The urban heat island effect is linked with thermal comfort and hence influences people's health conditions (Mavrogianni et al., 2011). In our study, we examine the heat index (HI) by using a multiple regression analysis that was first used by Steadman (1979) and again in many other recent studies (Yip et al., 2008; Mohan et al., 2014). The Steadman's HI is widely used by U.S. National Weather Service as an operational metric of thermal comfort that includes temperature and relative humidity together. It describes the perception of heat that a human body feels under the current weather. The calculation of HI is as follows (Rothfusz, 1990):

$$\begin{aligned} HI = {} & -42.379 + 2.04901523 * T + 10.14333127 * RH \\ & - 0.22475541 * T * RH - 0.00683783 * T^2 - 0.05481717 * RH^2 \\ & + 0.00122874 * T^2 * RH + 0.00085282 * T * RH^2 - 0.00000199 * T^2 * RH^2 \end{aligned} \quad (4)$$

where the HI is calculated in °F but has transferred to °C for consistency, T is the dry-bulb temperature, and RH is the relative humidity. In our study, the HI was calculated based on 2-m temperature and 2-m relative humidity from WRF outputs.

3. Results

3.1. Model validation: near-surface temperature and wind

The near-surface temperature above ground is calculated using the Monin-Obukhov similarity theory (Monin and Obukhov, 1954) as:

$$T_2 = T_s + (T_a - T_s)\frac{U}{U^*} \quad (5)$$

where T_s is the surface temperature, T_a is the 1st layer model level, $U*$ is the friction velocity at 2 m and U is the velocity at the 1st model level. The CTL simulated 2-m air temperature and 10-m horizontal wind were evaluated against values from 6 observation stations (Fig. 3) over the entire simulation period (August 21st to 27th, 2021). The results present that the CTL agreeably simulated the variations of near-surface temperature and 10-m

Table 5
Name, location, and land-use class of observational stations used in this study (from MesoWest website).

Station	Station name	Lat., Lon. (°N, °W)	Land-use classification in WRF
1	E1098 Chicago	41.88183, −87.66333	LCZ 2, compact mid-res
2	KMDW Chicago Midway Airport	41.78417, −87.75528	LCZ 8, large low-res
3	KORD Chicago O'Hare Airport	41.97972, −87.90444	LCZ 6, open low-res
4	KPWK Chicago Wheeling	42.12083, −87.90472	LCZ 6, open low-res
5	DeKalb Taylor Municipal Airport	41.93381, −88.70657	Rural (cropland)
6	Aurora Municipal Airport	41.77132, −88.48147	Rural (cropland)

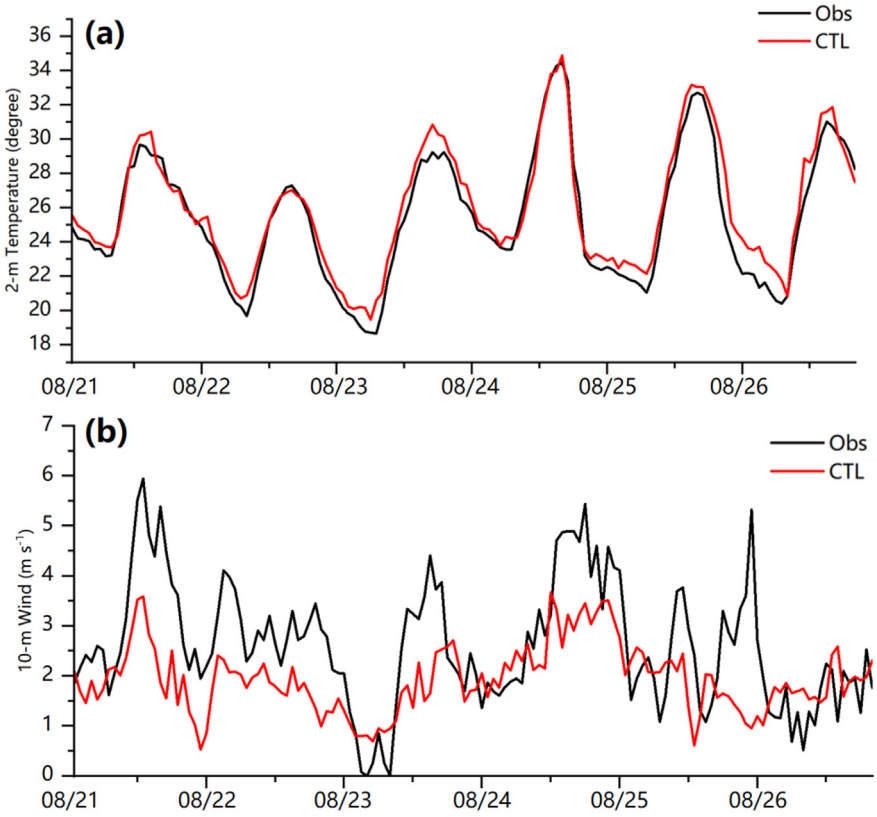

Fig. 3. Time series of (a) 2-m temperature (in °C) and (b) 10-m wind (in m s^{-1}) from observations (black) and CTL simulation (red) averaged across 6 weather stations between August 21–27th. The x-axis uses the local standard time (LST).

horizontal wind (Fig. 3). The mean bias error (MBE) of CTL compared with 6 observational stations is 1.4 °C over the entire simulated period. The simulated 2-m temperature averaged across 6 observational stations shows a warm bias at night. These biases were the systematic biases of the model and were identified by several earlier studies (Lee et al., 2011; Kim et al., 2013; Chen et al., 2014; Giovannini et al., 2014; Janicke et al., 2017; Wang et al., 2022). Furthermore, compared to BEP, the air conditioning systems for indoor cooling that are recognized in the BEP + BEM scheme as anthropogenic heat release produce more heat to be released into the atmosphere (Ribeiro et al., 2020). As a result, the urbanized regions are warmer at night than they are in the BEP experiments (Ribeiro et al., 2020). For wind speed, the CTL captures this variation in wind speed, although the speed is lower than that in the observation during afternoon hours. The low bias in wind speed is possibly due to misclassifications that could exist between a grid cell's land-use type and a station's footprint. Several of the stations, even those within CMA, are enclosures over relatively flat terrain, which a multi-layer parameterization cannot capture at the same scale. Further studies involving high-quality input data with more detailed land use classification, more accurate information on urban canopy structure and on urban surface's physical/thermal characteristics; as well as higher horizontal model resolution are strongly recommended to perform better in urban simulations. The performance of CTL during the heat wave event (Aug 24th), as represented by MBE and RMSE compared to the urban and rural stations, is summarized in Table 6.

3.2. Impacts of roof strategies on near-surface temperature and UHII

Fig. 4a–f shows the impacts of cool roofs, green roofs, and solar panel roofs deployment on near-surface temperature. All experiments show a cooling effect during the daytime. For example, the CR reduces the near-surface temperature by 1.5 °C during the daytime over CMA, followed by a 1.2 °C decrease for GR and a 0.6 °C decrease for SPR. The pattern is different at night: the GR has a warming effect at nighttime (Fig. 4e, f, and g), and for the CR experiment, the near-surface temperature remains relatively unchanged at night (compared with CTL). The SPR experiment also shows slight nighttime warming at the south of the CMA. In general, the roofing mitigation strategies reduce the near-surface temperature during the daytime but become less effective at night. These findings are consistent with previous analyses by Scherba et al. (2011) over Chicago, Georgescu (2015) over California, Yang et al. (2016) over Houston, Texas, and Zonato et al. (2021) in an idealized case. The nighttime difference can be explained by the following mechanism: because the net radiative flux is larger in summer than in winter, the urban infrastructure can collect more heat flux during the day and release it during the night. Because the green roof has additional soil layers, it is able to store more heat during daytime compared to other roofs and release that energy at night, generating a warming impact. Moreover, when the incoming solar

Table 6
Summary of averaged mean bias error (MBE) and root mean square error (RMSE) between CTL and urban/rural observational stations for 2-m temperature and 10-m wind during day (0700–1900 LST), night (1900–0700 LST), and total during August 21–27th, 2021.

	Time	2-m temperature		10-m wind	
		MBE	RMSE	MBE	RMSE
Urban stations					
1, 2, 3, 4	Total	1.48	2.28	−1.67	2.11
	Day	0.24	1.63	−1.08	2.43
	Night	1.24	2.79	−0.59	1.74
Rural stations					
5, 6	Total	1.54	3.21	−0.64	1.66
	Day	0.16	2.40	−0.46	1.60
	Night	1.38	3.85	−0.18	1.71

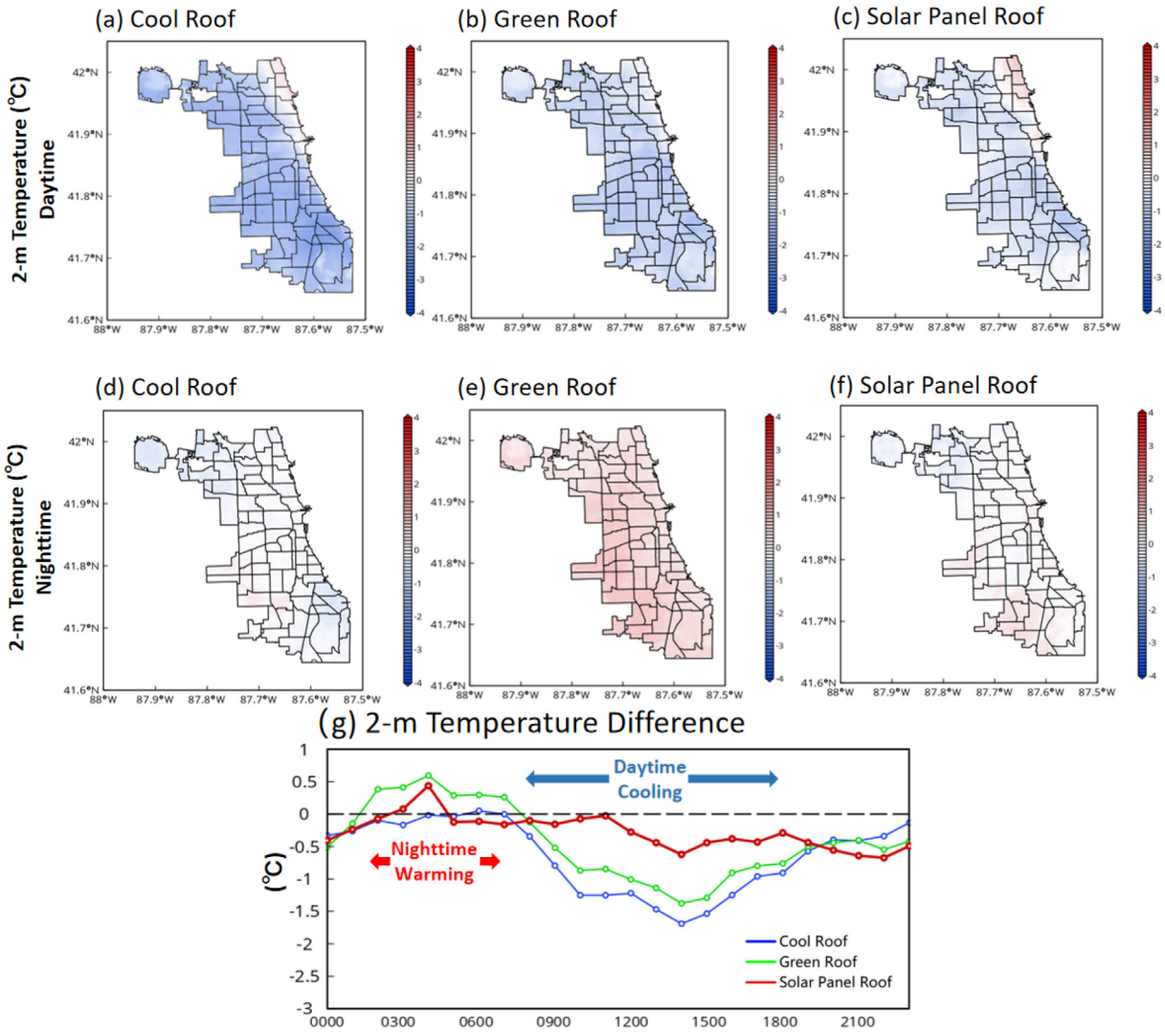

Fig. 4. The 6-day averaged 2-m temperature difference (minus CTL) for (a) Cool Roof, (b) Green Roof, and (c) Solar Panel Roof during daytime (1100–1700 LST). (d–f) show the difference during nighttime (0000–0600 LST). (g) shows the diurnal cycle of 2-m temperature difference between cool roof (blue), green roof (green), and solar panel roof (red) to CTL. Units are °C.

radiation is missing at night, the vertical mixing over the urban layer is inadequate, leading to stable air temperature evolution (Poulos et al., 2002; Yang et al., 2016). The performance of green roofs and solar panel roofs has been tested in wintertime by Zonato et al. (2021) and shows that the green roof and solar panel roof are capable of increasing the near-surface temperature and hence reducing energy consumption.

In addition, the implementation of roofing technology could affect different urban land-use categories. Table 7 presents peak heat mitigation for different urban land-use categories. The peak daily heat island mitigation is calculated by using the peak 2-m temperature from each roofing experiment minus the 2-m temperature from CTL at the same local standard time (LST) during the heatwave event (Aug 24th), then calculating the area-averaged over the black box in Fig. 1. As the urban fraction changes (from LCZ 6, 8, 3), the mitigation of peak heat island changes too, for all of the three roofing technologies. Overall, the CR has the best mitigation effect on near-surface temperature over these three major urban categories, which is further supported by Zonato et al. (2021). Fig. 5 quantifies the impact of different rooftops on UHII during daytime. For CTL, the mean daytime 2-m temperature increases with the increases in FRC_URB, implying the connection between UHII and urban development level. The CR, on the other hand, shows that temperature tends to decrease as the urban fraction increases, indicating that it is an effective rooftop mitigation strategy. The UHII in CTL is 1.91 °C, followed by −0.27 °C for CR, 0.40 °C for GR, and 0.98 °C for SPR.

Table 7
Peak daily heat island mitigations (°C) based on 2-m temperature averaged over Chicago metropolitan area for different land use categories.

LCZ land-use category	Cool roof	Green roof	Solar panel roof
LCZ 6	3.8	2.2	2.1
LCZ 3	3.7	2.4	2.2
LCZ 8	4.4	2.9	2.7

3.3. Heat index

Fig. 6 presents the 6-day averaged HI difference for different roof experiments. It shows that the CR experiment lowers the HI more than the GR and SPR experiments do. The reason that the GR condition does not significantly decrease the HI is that there is higher evaporation during daytime and a lower horizontal wind speed, which is further explained by Sharma et al. (2016) over the Chicago area. The CR slightly lowers the HI by 1.4 °C, followed by a 0.8 °C decrease for SPR and a 0.3 °C decrease for

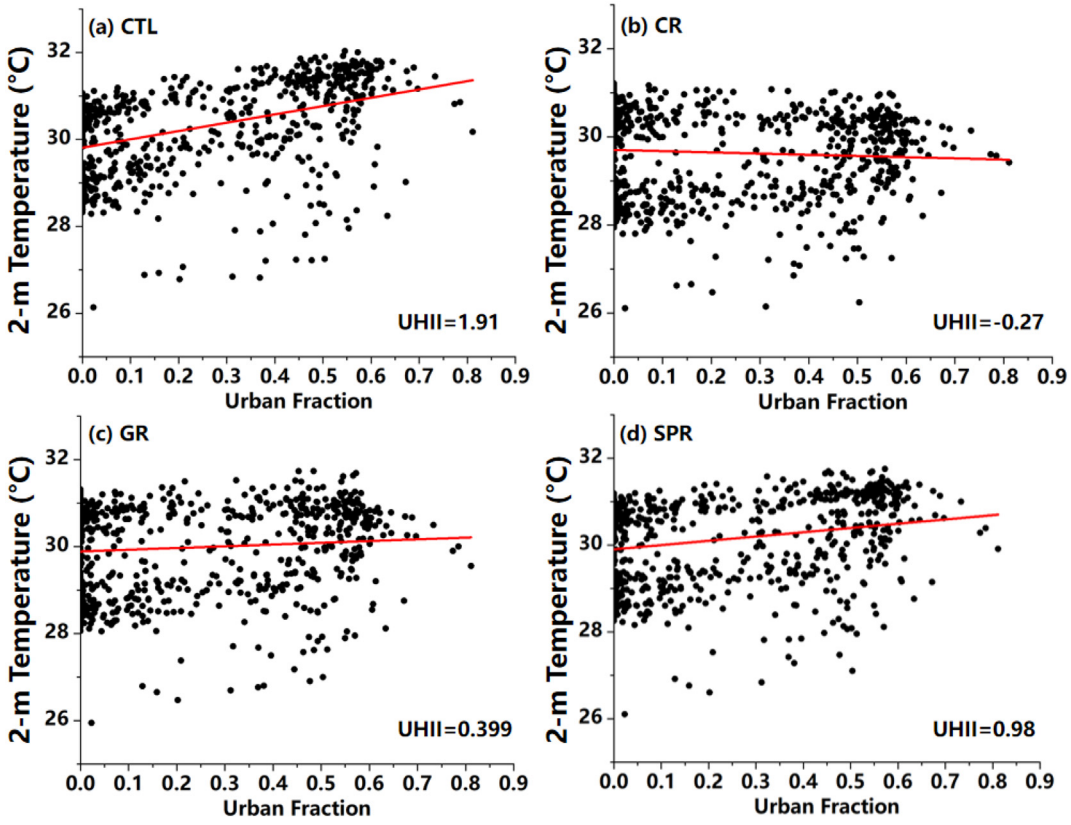

Fig. 5. Relationship between daytime 2-m temperature (°C) and the urban fraction (dimensionless) with linear fitting (red line) across solid black box area in Fig. 2b. The unit for urban heat island intensity (UHII) is °C.

GR. Fig. 7 presents the hours of HI difference that have temperatures >32.2 °C (90 °F) during the heatwave event (August 24, 2021). The results show that for CR, the HI hours that exceed 32.2 °C are noticeably reduced over the south of CMA but slightly increased over the northern coastline. The GR and SPR, however, had less effect on the hours of HI that exceed 32.2 °C over most of CMA. For near-surface relative humidity, all tests indicate an increase over the CMA, with the CR increasing the relative humidity the most (Fig. 8).

Besides numerical simulations, urban canopy parameters such as sky view factor (SVF) and frontal area index (FAI) also impact the UHI effect (Chen and Ng, 2011; He et al., 2019). SVF is defined as the ratio between the radiation received by a planar surface from the sky to the radiation released to the total hemispheric region, which is also adimensional. Over urban areas, the value of SVF reduces with the increase of sky that is blocked by the building, and hence more longwave radiation is trapped inside the urban canopy. Consequently, a less SVF is commonly associated with a more intense UHI. (He et al., 2019). The FAI calculates the frontal area per unit horizontal area (Burian et al., 2002a,b). The lower FAI leads to a higher local wind speed and subsequently a stronger mitigation impact on the UHI effect (Burian et al., 2002a,b; Chen and Ng, 2011). Even though the impact of these two factors on UHI is beyond the scope of this research, more comprehensive knowledge can be found in Chen and Ng (2011).

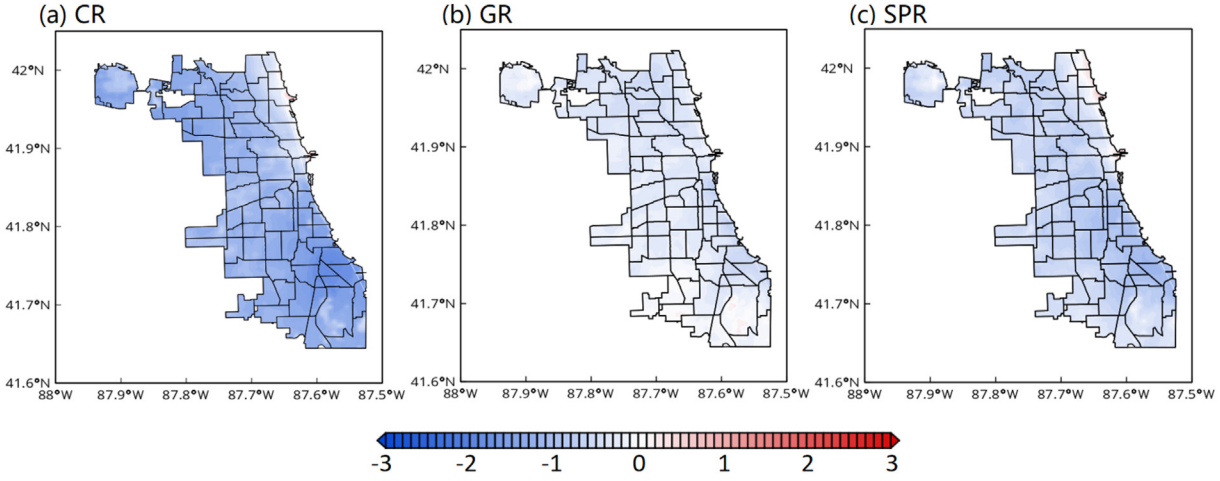

Fig. 6. The 6-day averaged heat index difference (minus CTL) for (a) CR, (b) GR, and (c) SPR. Units are °C.

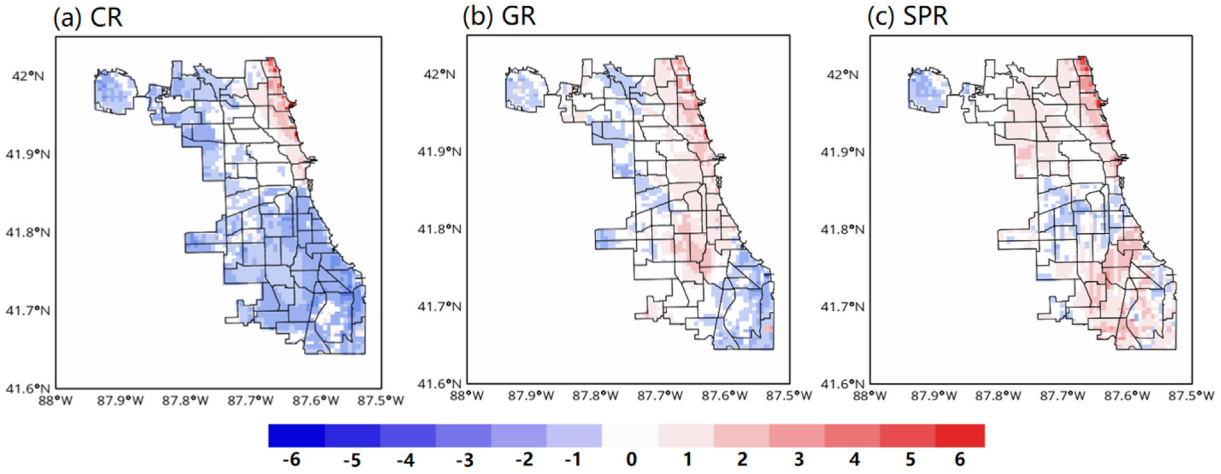

Fig. 7. Hours of heat index difference that are >32.2 ˚C (90 ˚F) during the heatwave event (August 24, 2021) for (a) CR, (b) GR, and (c) SPR over CMA.

3.4. Impacts of roof strategies on boundary layer

To further illustrate the impact of CR, GR, and SPR on the boundary layer, we present the time series of differences in vertical profiles of relative humidity, horizontal wind, and temperature by subtracting the results from the CTL simulation. The reduction of temperature in atmospheric up to 1.4–1.6 km was observed during the heatwave event (Aug 24th) when roofs are applied (Fig. 9 a–c). The maximum reduction in the atmospheric temperature occurred when the CR was applied. For horizontal wind, the decrease in horizontal wind due to the reduced vertical mixing of momentum was detected below 1 km of the atmosphere and the increase above 1 km during the heatwave event (Aug 24th), especially over CR and GR. After the vertical mixing is decreased, the airflow over higher levels with stronger wind speed was less penetrated into lower-level air with less wind speed which is due to less momentum shift from higher levels to lower levels, so that the wind speed above urban canopy level was reduced when roofs are applied, generating stronger (weaker) wind speed in higher (lower) levels. The study by Owinoh et al. (2005) and Zilitinkevich et al. (2006) shows a detailed discussion of the dynamics. For relative humidity, it is increased due to the reduced temperature which is capable of lower the saturation vapor pressure in CR and SPR. The increase in relative humidity in GR can be attributed to higher evaporation and lower horizontal wind speed.

These results indicate that advanced roofing technology mainly mitigates the air temperature but may exacerbate relative humidity. This exacerbation is related to effects induced by changes in vertical mixing. Studies have shown that after the deployment of cool roofs and green roofs, the sensible heat flux decreases, which in turn increases the stability of the atmosphere and hence decreases the vertical mixing over the city (Li et al., 2014; Sharma et al., 2016). When vertical mixing weakens, it takes more time to establish the internal boundary layer when air flows develop from rural to urban regions. Hence, the atmosphere is less affected by the surface but more influenced by advection coming from upwind surfaces. Consequently, the weaker mixing has a stronger advective effect on urban regions. Finally, the stronger moisture advection in the air from rural regions induces an increase in humidity over urban areas after installation of advanced roofs (Li et al., 2014; Sharma et al., 2016).

3.5. Surface energy balance

Fig. 10 displays 6-day averaged diurnal cycle of surface latent heat flux (Fig. 10a), sensible heat flux (Fig. 10b), net shortwave radiation (Fig. 10c), net longwave radiation (Fig. 10d), and ground heat flux (Fig. 10e) from all experiments. Positive values indicate incoming heat flux to the surface, while negative values indicate outgoing heat flux to the atmosphere. Fig. 10a shows that the CR and SPR decrease the latent heat flux, with the peak reduced by 50 W m^{-2} and 30 W m^{-2}, respectively. The GR, on the other hand, decreases the sensible heat flux by building the shade and re-separates the available energy to increase latent heat flux by 80 W m^{-2} via evapotranspiration, hence, reducing the temperature. For sensible heat flux (Fig. 10b), the CR reduces the peak of sensible heat flux the most

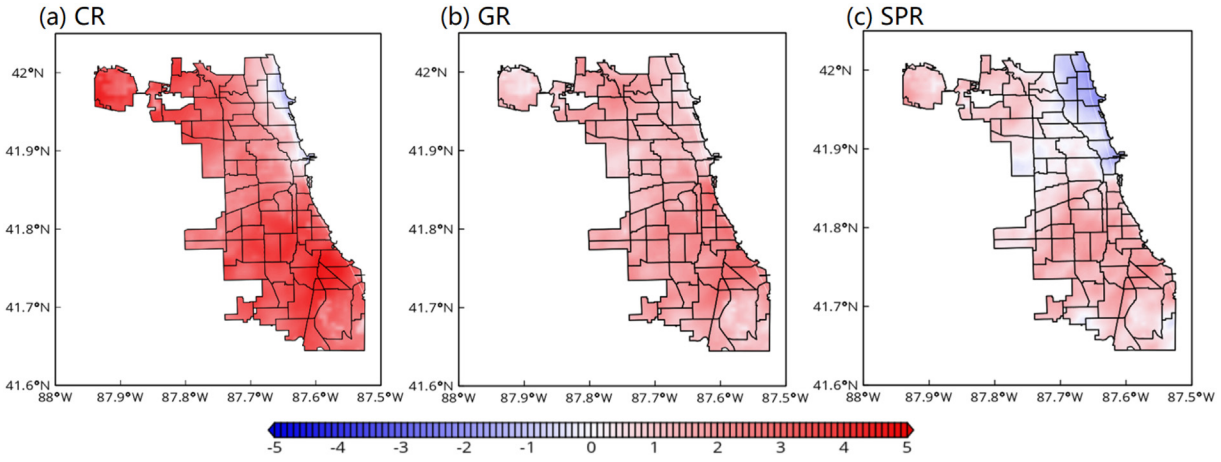

Fig. 8. The 6-day averaged 2-m relative humidity differences for (a) CR, (b) GR, and (c) SPR. Values are percentages.

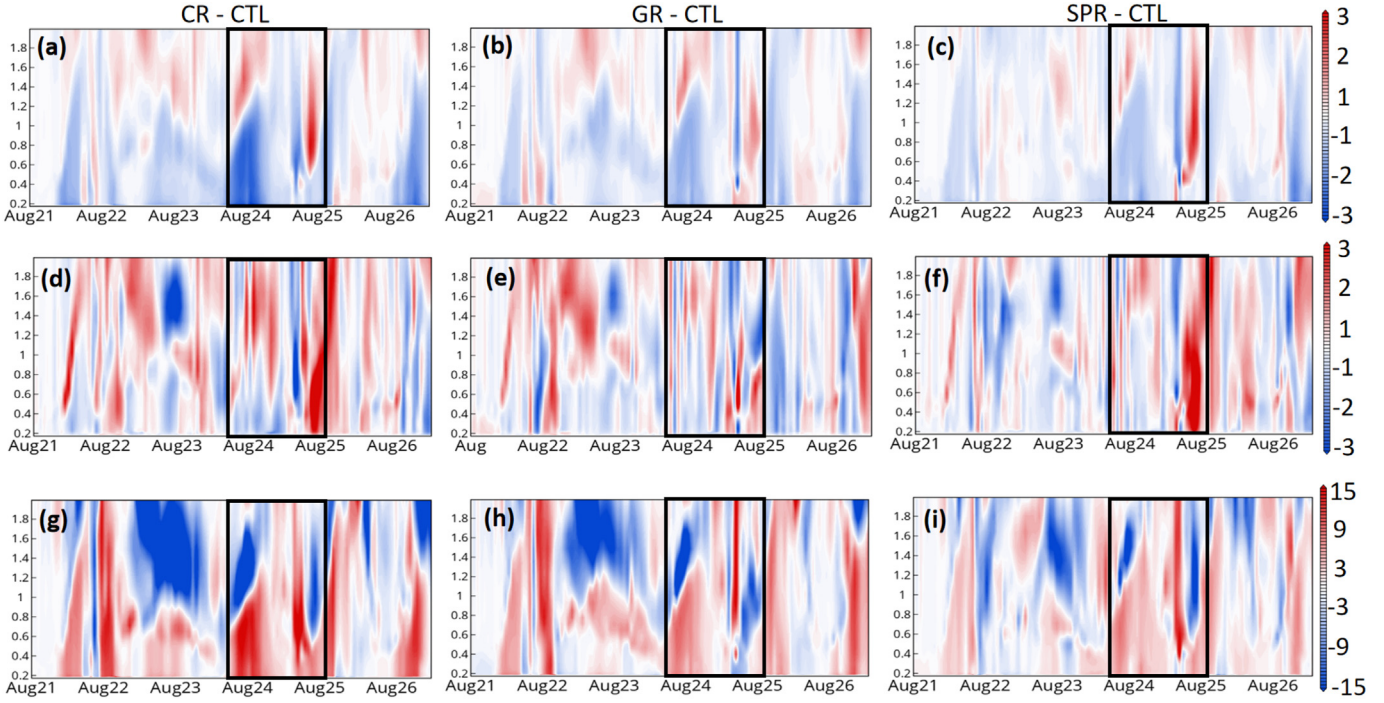

Fig. 9. Vertical profile differences between CTL and CR, GR, and SPR on (a–c) temperature (°C), (d–f) horizontal wind (m s^{-1}), and (g–i) relative humidity (%) for CMA-averaged from August 21–27th. Black box indicates the heatwave event (Aug 24th).

(155 W m^{-2}), followed by GR (103 W m^{-2}) and SPR (84 W m^{-2}). Consequently, these roofs are able to limit the transmission of heat into urban interior and the broader environment by decreasing sensible heat flux, so that the near-surface temperature and the cooling consumption are reduced. For net radiative flux, the CR and SPR share a similar tendency on both shortwave and longwave radiation, indicating that the reflective effect in CR and the absorption by photovoltaic cells in SPR are similar. The GR can receive slightly more net shortwave radiation during afternoon hours. The ground heat flux decreased in CR, GR, and SPR during daytime compared with CTL, indicating less heat flows into the building.

3.6. Impacts on cooling energy demand

This section addresses the summertime regional impacts of cool roofs, green roofs, and solar panel roofs deployment on AC energy consumption. Fig. 11a–c shows the AC energy consumption differences (MW km^{-2}) between CTL and the three roof experiments (CR, GR, and SPR), and Fig. 11d shows the diurnal cycle of CMA AC consumption (MW km^{-2}). Overall, all three roofing strategies reduce the AC energy consumption of the entire CMA. In particular, CR significantly decreases the AC energy consumption (Fig. 11a) because CR has the least heat transmission into the urban canopy layer compared to GR and SPR, especially during the daytime when the air temperature and the AC demand are both at the highest. The daily average reduction of AC energy consumption is 16.6 % by CR, 14.0 % by GR, and 7.6 % by SPR, similar to what Salamanca et al. (2016) found over Phoenix and Tucson (13–14 % by CR and 8.7–11 % by SPR). In contrast, Salamanca et al. (2016), who observed that partially covered solar panel roofs reduce AC consumption during the day but increase cooling energy demand at night (because solar panels receive less incoming solar radiation during the day, hence it permits less radiative cooling at night), our study finds the AC consumption is reduced during both daytime and nighttime over CMA by all roofing strategies (Fig. 11d). This may be because more heat is conducted into the building from the rooftop during the day and released at night when the rooftop is partially covered by solar panels in Salamanca's study. Other possibilities also include various city morphologies (i.e. building fraction, building sizes). Since Phoenix's local cooling energy demand is higher than Chicago's (Hong et al., 2009), the disparity in local cooling energy demand between CMA and Phoenix may also be a significant contributing factor.

While the SPR shows the smallest savings on AC consumption, it generates electricity. A detailed description of electricity production by solar photovoltaic panels is presented by Zonato et al. (2021). We assume the conversion efficiency of the solar photovoltaic panels to be 0.19. The electricity production by solar panels starts at 0600 LST and peaks at 1300 LST at 10.7 MW km^{-2}, which almost overcomes the cooling energy demand (orange line, Fig. 11d). If all the power generated by solar panel roofs is used for cooling, we may expect a cooling energy savings of 46.7 % on a daily average in the SPR experiment, which is considerably more than the cooling energy savings in CR and GR.

4. Discussion and conclusions

This study evaluates the impacts of city-scale deployment of cool roofs, green roofs, and rooftop solar panels on near-surface temperatures and cooling energy demand using a fully coupled modeling system consisting of an urban-resolving regional climate model during a summertime heatwave event over CMA. The results of the study can inform development and implementation of sustainable approaches that decrease the direct effects of urbanization, lower summertime cooling energy demand, and help minimize greenhouse gas emissions in the long term over CMA.

We find that the distribution of cool roofs, green roofs, and solar panel roofs reduces the near-surface temperature and AC consumption demand at the city scale, especially during daytime when the air temperature is the highest. In particular, cool roofs can reduce the near-surface temperature by 1.5 °C, followed by 1.2 °C for green roofs and 0.6 °C for solar panel roofs. In line with Georgescu et al. (2014) and Sharma et al. (2016), green roofs have a slight nighttime warming effect because the rooftop soil layers accumulate extra solar radiation during the daytime and discharge it at night. The peak reduction in the daily urban heat island is 3.9 °C for cool roofs, 2.5 °C for green roofs, and 2.3 °C for solar panel roofs. Examination of the effect of urban fraction was revealing: The cool roof experiment was the only one where the 2-m temperature trended

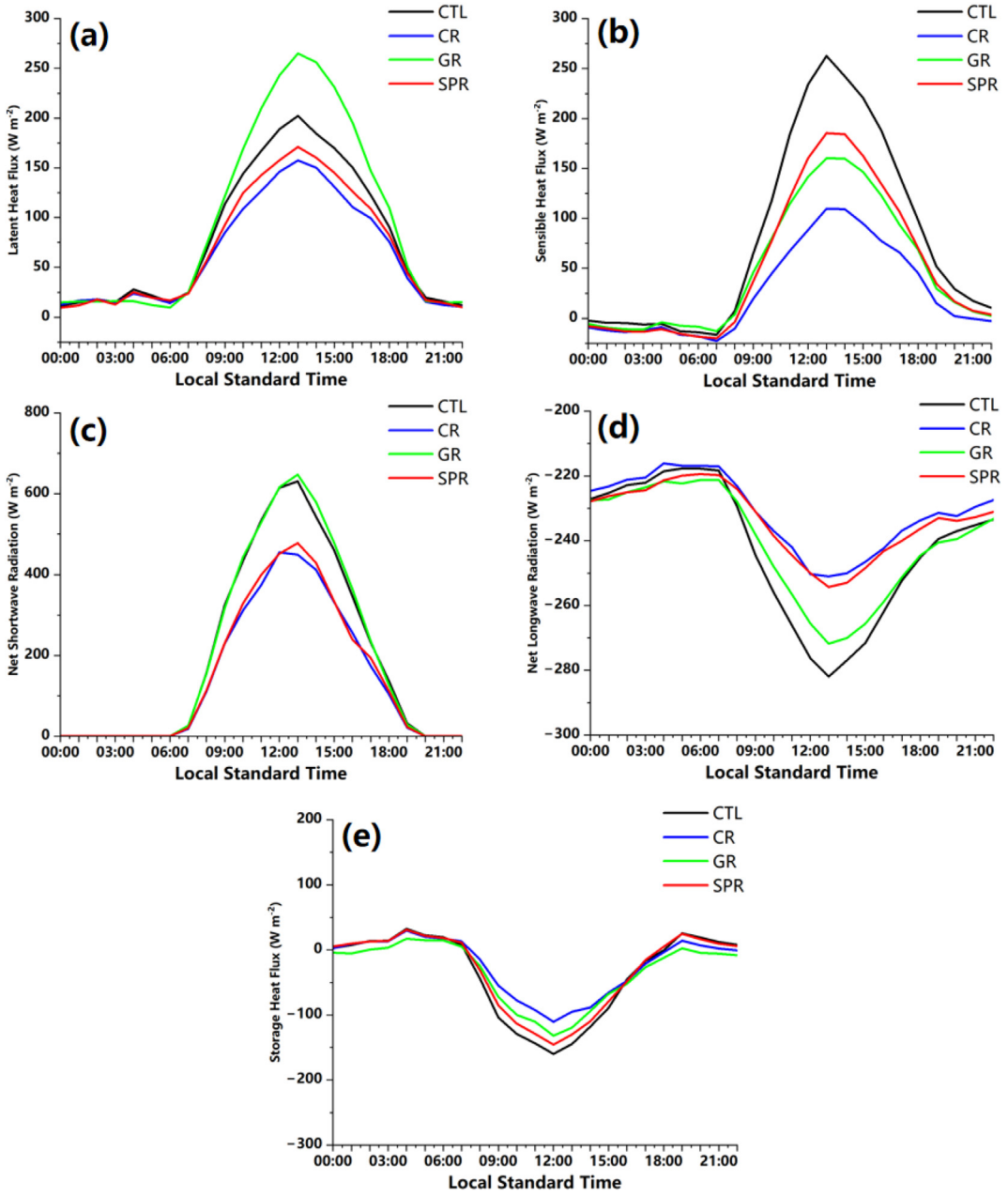

Fig. 10. Diurnal cycle of energy balance terms for August 21–27th, 2021: (a) latent heat flux, (b) sensible heat flux, (c) net shortwave radiation, (d) net longwave radiation, and (e) ground heat flux for CTL (black), Cool Roof (blue), Green Roof (green), and Solar Panel Roof (red).

down as the urban fraction increased, indicating the cool roof is the most effective mitigation strategy among these three rooftop options. The reduction in heat index is relatively small, especially for green roofs because of the increase in humidity. The peak daily heat island mitigations based on 2-m temperature averaged is over LCZ 8, which does not own the largest urban fraction. However, the idealized two-dimensional experiments by Zonato et al. (2021) show that the mitigation effect from roofing on air temperature varies almost linearly with the building surface to total surface fraction during summer time. The mitigation effect is also higher for low buildings, with a nonlinear decrease in the impact with building heights. Additionally, they draw the conclusion that the urban configuration with the lowest buildings and the highest building area to total area ratio shows the highest effect of the roofing mitigation. We will keep investigating this by designing more experiments based on different urban fractions and building heights in real-time simulation in the future. The deployment of the roof surface also influences the structure of the boundary layer during the heatwave event. The temperature, horizontal winds, and relative humidity in the lower atmosphere alter due to the mitigation of UHI from rooftops.

Because all the roofing strategies offer cooling effects, they reduce AC consumption. For example, the citywide cooling energy consumption can be reduced by 16.6 %, 14.0 %, and 7.6 %, when cool roofs, green roofs, and solar panel roofs are deployed, respectively. Although solar panel roofs show the smallest reduction in energy consumption, if we assume that all electricity production can be applied to cooling demand, we can expect almost a savings of almost half (46.7 %) on cooling energy demand.

Several trade-offs must be considered when choosing between cool roofs, green roofs, and solar panel roofs as artificial mitigation techniques. The large-scale deployment of cool roofs has the best potential for cooling effects and cooling energy saving; they cost less than the other two technologies; and they do not require additional water. However, the performance of cool roofs can be misleading in perturbation experiments because the

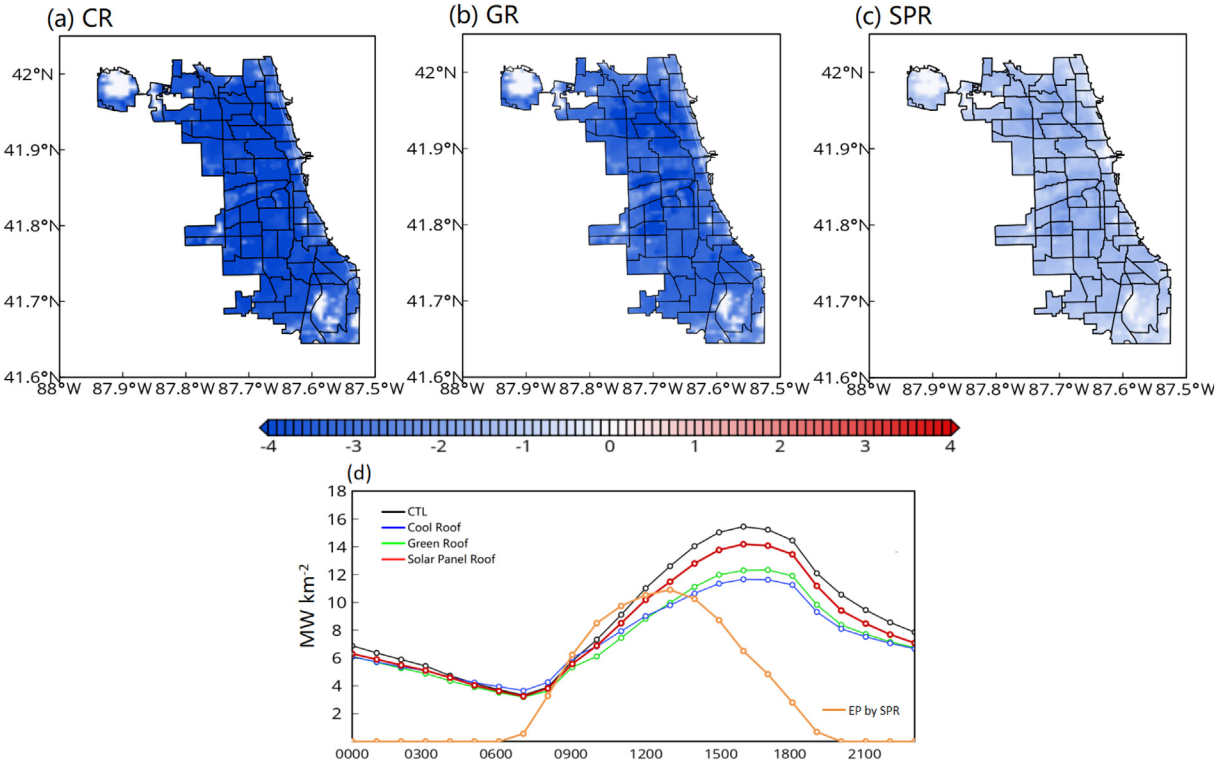

Fig. 11. Daytime air-conditioning electricity consumption change (compared to CTL) due to (a) Cool Roof, (b) Green Roof, and (c) Solar Panel Roof over 6-day extreme heat period (August 21–27, 2021) across CMA. (d) Diurnal cycle of simulated air-conditioning electricity consumption for CTL (black), cool roof (blue), green roof (green), and solar panel roof (red) and the electricity production generated by solar panel roof (EP by SPR, orange). Unit in MW km^{-2}.

roof albedo can decrease over time because of weathering and the accumulation of dirt on the surface (Bretz and Akbari, 1997). Green roofs increase water use and local humidity, but they can add a considerable amount of vegetation to the urban environment, which has several potential co-benefits, and they can reduce pollutants through dry deposition and absorption of gaseous pollutants through leaf stomata (Yang et al., 2008; Nowak et al., 2014). However, purely from a heat mitigation perspective, we should also consider the warming effects such roofs have at night over urban areas (Georgescu et al., 2014; Sharma et al., 2016) and their minimal impact on reducing the heat index. Regarding the heat index, it is important to note that the current version of our model does not explicitly represent street vegetation, which can further mitigate heat exposure through shading at local scales (Mussetti et al., 2020). Solar photovoltaic panels are generally discussed in the context of reduced reliance on fossil fuels and hence global warming instead of in the context of local-scale heat mitigation. However, this study demonstrates that solar panels can be another effective mitigation method in the long term, thanks to their ability to generate considerable amounts of electricity, which can indirectly reduce net cooling energy demands. The ongoing scientific development in improving solar conversion efficiency of the panels may further add to this benefit in the future. It is important to also consider the trade-offs between urban heat mitigation and air quality (Li et al., 2014; Sharma et al., 2016), which we do not address in the present study.

Although we show that advanced roofing technologies are a productive way to mitigate urban temperature during a summer heatwave event, the efficacy of these mitigation methods would depend on the time of the year and is a function of the simplifications in the urban model. All urban characteristics (morphological, thermodynamic, radiative, aerodynamic, etc.) are difficult to accurately prescribe even at higher resolutions because of uncertainties in both observations and model parameterizations (Chen et al., 2012; Chakraborty et al., 2021; Qian et al., 2022). For instance, a city may possess a distinct morphology (i.e., building fraction, building sizes, etc.), whose impacts on urban micro-climate can deviate from those simulated by bulk parameterizations in the models, thus modulating the quantitative benefits derived for these rooftop strategies. A broader climatological study accounting for various seasons would require enormous computational time at 500-m resolution; such a study is beyond the scope of the current study but would be a consideration in the future. Another caveat from the model perspective is that although in BEP + BEM the anthropogenic heat flux is triggered by air conditioning, the heat exchanges between interior building and outside air, and heat release by equipment and people within the building, it doesn't include anthropogenic heat from traffic and industrial activities. We plan to conduct more tests in BEP + BEM with more realistic anthropogenic heat fluxes as the next step.

CRediT authorship contribution statement

Haochen Tan: Visualization; Investigation; Writing, Reviewing and Editing; Validation; Formal analysis.
Rao Kotamarthi: Conceptualization, Methodology, Funding acquisition.
Jiali Wang: Methodology; Reviewing and Editing.
Yun Qian: Supervision; Project administration;
TC Chakraborty: Investigation; Writing; Validation.

Data availability

Data will be made available on request.

Declaration of competing interest

The authors declare that they have no known competing financial interests or personal relationships that could have appeared to influence the work reported in this paper.

Acknowledgments

This study is supported by COMPASS-GLM, a multi-institutional project supported by the U.S. Department of Energy (DOE), Office of Science,

Office of Biological and Environmental Research as part of the Regional and Global Modeling and Analysis (RGMA) program, Multi-sector Dynamics Modeling (MSD) program, and Earth System Model Development (ESMD) program. We also acknowledge support from the CROCUS project funded by DOE BER under contract number DE-FOA-0002581. Computational resources are provided by the DOE-supported National Energy Research Scientific Computing Center and Argonne Leadership Computing Facility. All the calculations are done using the NCAR Command Language (version 6.6.2) (2019, Boulder, Colorado: UCAR/NCAR/CISL/TDD, https://doi.org/10.5065/D6WD3XH5). MesoWest datasets were used in this study (http://mesowest.utah.edu).

References

Akbari, H., Menon, S., Rosenfeld, A., 2009. Global cooling: increasing world-wide urban albedos to offset CO2. Clim. Chang. 94, 275–286. https://doi.org/10.1007/s10584-008-9515-9.

Bou-Zeid, E., Meneveau, C., Parlange, M.B., 2004. Large-eddy simulation of neutral atmospheric boundary layer flow over heterogeneous surfaces: blending height and effective surface roughness. Water Resour. Res. 40, W02505. https://doi.org/10.1029/2003WR002475.

Bou-Zeid, E., Parlange, M.B., Meneveau, C., 2007. On the parameterization of surface roughness at regional scales. J. Atmos. Sci. 64, 216–227. https://doi.org/10.1175/JAS3826.1.

Bretz, S.E., Akbari, H., 1997. Long-term performance of high-albedo roof coatings. Energy. Build. 25 (2), 159–167. https://doi.org/10.1016/S0378-7788(96)01005-5.

Brousse, O., Martilli, A., Foley, M., Mills, G., Bechtel, B., 2016. WUDAPT, an efficient land use producing data tool for mesoscale models? Integration of urban LCZ in WRF over Madrid. Urban Clim. 17, 116–134. https://doi.org/10.1016/j.uclim.2016.04.001.

Burian, S.J., Brown, M.J., Linger, S.P., 2002. Morphological Analyses Using 3D Building Databases. 74. Los Alamos National Laboratory, Los Angeles, California.

Burian, S.J., Brown, M.J., Linger, S.P., 2002. Morphological Analyses Using 3D Building Databases, p. 74 Los Angeles, California.

Chakraborty, T.C., Lee, X., Ermida, S., Zhan, W., 2021. On the land emissivity assumption and Landsat-derived surface urban heat islands: a global analysis. Remote Sens. Environ. 265, 112682. https://doi.org/10.1016/j.rse.2021.112682.

Chen, F., Dudhia, J., 2001. Coupling an advanced land surface–hydrology model with the Penn State–NCAR MM5 modeling system. Part I: model implementation and sensitivity. Mon. Weather Rev. 129 (4), 569–585.

Chen, F., Bornstein, R., Grimmond, S., Li, J., Liang, X., Martilli, A., Miao, S., Voogt, J., Wang, Y., 2012. Research priorities in observing and modeling urban weather and climate. Bull. Am. Meteorol. Soc. 93 (11), 1725–1728. https://doi.org/10.1175/BAMS-D-11-00217.1.

Chen, F., Yang, X., Zhu, W., 2014. WRF simulations of urban heat island under hot-weather synoptic conditions: the case study of Hangzhou City, China. Atmos. Res. 138 (1), 364–377 doi:j.atmosres.2013.12.005.

Chen, K., Newman, A.J., Huang, M., Coon, C., Darrow, L.A., Strickland, M.J., Holmes, H.A., 2022. Estimating heat-related exposures and urban heat island impacts: a case study for the 2012 Chicago heatwave. GeoHealth 6, e2021GH000535. https://doi.org/10.1029/2021GH000535.

Chen, L., Ng, E., 2011. Quantitative urban climate mapping based on a geographical database: a simulation approach using Hong Kong as a case study. Int. J. Appl. Earth Obs. Geoinf. 13 (4), 586e594.

Ching, J., Mills, G., Bechtel, B., See, L., Feddema, J., Wang, X., Ren, C., Brousse, O., Martilli, A., Neophytou, M., Mouzourides, P., Stewart, I., Hanna, A., Ng, E., Foley, M., Alexander, P., Aliaga, D., Niyogi, D., Shreevastava, A., Bhalachandran, P., Masson, V., Hidalgo, J., Fung, J., Andrade, M., Baklanov, A., Dai, W., Milcinski, G., Demuzere, M., Brunsell, N., Pesaresi, M., Miao, S., Mu, Q., Chen, F., Theeuwes, N., 2018. WUDAPT: an urban weather, climate, and environmental modeling infrastructure for the anthropocene. Bull. Am. Meteorol. Soc. 99 (9), 1907–1924. https://doi.org/10.1175/BAMS-D-16-0236.1.

Davies, F., Middleton, D.R., Bozier, K.E., 2007. Urban air pollution modelling and measurements of boundary layer height. Atmos. Environ. 41, 4040–4049. https://doi.org/10.1016/j.atmosenv.2007.01.015.

de Munck, C.S., Lemonsu, A., Bouzouidja, R., Masson, V., Claverie, R., 2013. The GREENROOF module (v7.3) for modelling green roof hydrological and energetic performances within TEB. Geosci. Model Dev. 6 (6), 1941–1960. https://doi.org/10.5194/gmd-6-1941-2013.

Demuzere, M., Hankey, S., Mills, G., Zhang, W.W., Lu, T.J., Bechtel, B., 2020. Combining expert and crowd-sourced training data to map urban form and functions for the continental US. Sci. Data 7, 264. https://doi.org/10.6084/m9.figshare.12599966.

Demuzere, M., Argüeso, D., Zonato, A., Kittner, J., 2022. W2W: a python package that injects WUDAPT's local climate zone information in WRF. J. Open Source Softw. 7 (76), 4432. https://doi.org/10.21105/joss.04432.

Dominguez, A., Kleissl, J., Luvall, J.C., 2011. Effects of solar photovoltaic panels on roof heat transfer. Sol. Energy 85, 2244–2255. https://doi.org/10.1016/j.solener.2011.06.010.

Dudhia, J., 1989. Numerical study of convection observed during the winter monsoon experiment using a mesoscale two-dimensional model. J. Atmos. Sci. 46, 3077–3107.

Ek, M.B., Mitchell, K.E., Lin, Y., Rogers, E., Grunmann, P., Koren, V., Gayno, G., Tarpley, J.D., 2003. Implementation of Noah land surface model advances in the National Centers for Environmental Prediction operational mesoscale Eta model. J. Geophys. Res. Atmos. 108 (2003). https://doi.org/10.1029/2002jd003296.

Foley, M., 2015. Chicago WUDAPT Level 0 training data is licensed under CC-BY-NC-SA 4.0. Available at www.wudapt.org/cities/raw-training-area-download/.

Georgescu, M., 2015. Challenges associated with adaptation to future urban expansion. J. Clim. 28, 2544–2563. https://doi.org/10.1175/JCLI-D-14-00290.1.

Georgescu, M., Moustaoui, M., Mahalov, A., Dudhia, J., 2013. Summer-time climate impacts of projected megapolitan expansion in Arizona. Nat. Clim. Change 3, 37–41. https://doi.org/10.1038/nclimate1656.

Georgescu, M., Morefield, P.E., Bierwagen, B.G., Weaver, C.P., 2014. Urban adaptation can roll back warming of emerging megapolitan regions. Proc. Natl. Acad. Sci. U. S. A. 111, 2909–2914. https://doi.org/10.1073/pnas.1322280111.

Giovannini, L., Zardi, D., de Franceschi, M., Chen, F., 2014. Numerical simulations of boundary-layer processes and urban-induced alterations in an alpine valley. Int. J. Climatol. 34 (4), 1111–1131. https://doi.org/10.1002/joc.3750.

Gutiérrez, E., Martilli, A., Santiago, J.L., González, J.E., 2015. A mechanical drag coefficient formulation and urban canopy parameter assimilation technique for complex urban environments. Bound.-Layer Meteorol. 157 (2), 333–341. https://doi.org/10.1007/s10546-015-0051-7.

Hammerberg, K., Brousse, O., Martilli, A., Mahdavi, A., 2018. Implications of employing detailed urban canopy parameters for mesoscale climate modelling: a comparison between WUDAPT and GIS databases over Vienna, Austria. Int. J. Climatol. 38, e1241–e1257. https://doi.org/10.1002/joc.5447.

Harris, L., Kotamarthi, V.R., 2005. The characteristics of the Chicago lake breeze and its effects on trace particle transport: results from an episodic event simulation. J. Appl. Meteor. 44, 1637–1654.

He, X., Li, Y., Wang, X., Chen, L., Yu, B., Zhang, Y., Miao, S., 2019. High-resolution dataset of urban canopy parameters for Beijing and its application to the integrated WRF/urban modelling system. J. Clean. Prod. 208, 373e383.

Hong, S.Y., Lim, J.O.J., 2006. The WRF single-moment 6-class microphysics scheme (WSM6). J. Korean Meteor. Soc. 42, 129–151.

Hong, T.Z., Sartor, D., Mathew, P., Yazdanian, M., 2009. Comparison of HVAC simulations between EnergyPlus and DOE-2.2 for data centers. ASHRAE Transcations. https://escholarship.org/content/qt2dq2w3b3/qt2dq2w3b3.pdf?t=lnqp8p.

Jaffal, I., Ouldboukhitine, S.E., Belarbi, R., 2012. A comprehensive study of the impact of green roofs on building energy performance. Renew. Energy 43, 157–164. https://doi.org/10.1016/j.renene.2011.12.004.

Janicke, B., Meier, F., Fenner, D., Fehrenbach, U., Holtmann, A., Scherer, D., 2017. Urbanrural differences in near-surface air temperature as resolved by the Central Europe refined analysis (CER): sensitivity to planetary boundary layer schemes and urban canopy models. Int. J. Climatol. 37 (4), 2063–2079. https://doi.org/10.1002/joc.4835.

Janjic, Z.I., 2002. Nonsingular Implementation of the Mellor-Yamada Level 2.5 Scheme in the NCEP Mesomodel. NCEP Office Note. No. 437 61pp.

Kim, Y., Sartelet, K., Raut, J.C., Chazette, P., 2013. Evaluation of the weather research and forecast/urban model over greater Paris. Bound.-Layer Meteorol. 149 (1), 105–132. https://doi.org/10.1007/s10546-013-9838-6.

Kong, F., Yan, W., Zheng, G., Yin, H., Cavan, G., Zhang, W., Zhang, N., Cheng, L., 2016. Retrieval of three-dimensional tree canopy and shade using terrestrial laser scanning (TLS) data to analyze the cooling effect of vegetation. Agric. For. Meteor. 217, 22–34. https://doi.org/10.1016/j.agrformet.2015.11.005.

Kumar, A., Chen, F., Barlage, M., Ek, M.B., Niyogi, D., 2014. Assessing impact of integrating MODIS vegetation data in the weather research and forecasting (WRF) model coupled to two different canopy-resistance approaches. J. Appl. Meteor. Clim. 53, 1362–1380. https://doi.org/10.1175/JAMC-D-13-0247.1.

Kusaka, H., Kondo, H., Kikegawa, Y., Kimura, F., 2001. A simple single-layer urban canopy model for atmospheric models: comparison with multi-layer and slab models. Bound.-Layer Meteorol. 101, 329–358. https://doi.org/10.1023/A:1019207923078.

Lee, S.H., Kim, S.W., Angevine, W.M., Bianco, L., McKeen, S.A., Senff, C.J., Trainer, M., Tucker, S.C., Zamora, R.J., 2011. Evaluation of urban surface parameterizations in the WRF model using measurements during the Texas air quality study 2006 field campaign. Atmos. Chem. Phys. 11 (5), 2127–2143. https://doi.org/10.5194/acp-11-2127-2011.

Li, D., Bou-Zeid, E., Oppenheimer, M., 2014. The effectiveness of cool and green roofs as urban heat island mitigation strategies. Environ. Res. Lett. 9, 055002. https://doi.org/10.1088/1748-9326/9/5/055002.

Li, H., Zhou, Y., Wang, X., Zhou, X., Zhang, H., Sodoudi, S., 2019. Quantifying urban heat island intensity and its physical mechanism using WRF/UCM. Sci. Total. Environ. 650, 3110–3119. https://doi.org/10.1016/j.scitotenv.2018.10.025.

Li, X.-X., Norford, L.K., 2016. Evaluation of cool roof and vegetations in mitigating urban heat island in a tropical city, Singapore. Urban. Clim. 16, 59–74. https://doi.org/10.1016/j.uclim.2015.12.002.

Liao, W., Liu, X., Li, D., Luo, M., Wang, D., Wang, S., Baldwin, J., Lin, L., Li, X., Feng, K., Hubacek, H., Yang, X., 2018. Stronger contributions of urbanization to heat wave trends in wet climates. Geophys. Res. Lett. 45 (20), 11310–11317. https://doi.org/10.1029/2018gl079679.

Livezey, R.E., Tinker, R., 1996. Some meteorological, climatological, and microclimatological considerations of the severe US heat wave of mid-July 1995. Bull. Am. Meteorol. Soc. 77, 2043–2054. https://doi.org/10.1175/1520-0477(1996)077<2043:SMCAMC>2.0.CO;2.

Ma, S., Goldstein, M., Pitman, A., Haghdadi, N., MacGill, I., 2017. Pricing the urban cooling benefits of solar panel deployment in Sydney, Australia. Sci Rep. 7, 43938. https://doi.org/10.1038/srep43938.

Martilli, A., Clappier, A., Rotach, M.W., 2002. An urban surface exchange parameterisation for mesoscale models. Bound.-Layer Meteorol. 104, 261–304. https://doi.org/10.1023/A:1016099921195.

Masson, V., Bonhomme, M., Salagnac, J.-L., Briottet, X., Lemonsu, A., 2014. Solar panels reduce both global warming and urban heat island. Front. Environ. Sci. 2, 1–10. https://doi.org/10.3389/fenvs.2014.00014.

Mavrogianni, A., Davies, M., Batty, M., Belcher, S.E., Bohnenstengel, S.I., Carruthers, D., Chalabi, Z., Croxford, B., Demanuele, C., Evans, S., Giridharan, R., Ye, Z., 2011. The

comfort, energy and health implications of London's urban heat island. Build. Serv. Eng. Res. Technol. 32, 35–52. https://doi.org/10.1177/0143624410394530.
McRae, I., Freedman, F., Rivera, A., Li, X.W., Dou, J.J., Cruz, I., Ren, C., Dronova, I., Fraker, H., Bornstein, R., 2020. Integration of the WUDAPT, WRF, and ENVI-met models to simulate extreme daytime temperature mitigation strategies in San Jose, California. Build. Environ. 184, 107180. https://doi.org/10.1016/j.buildenv.2020.107180.
Millstein, D., Menon, S., 2011. Regional climate consequences of large-scale cool roof and photovoltaic array deployment. Environ. Res. Lett. 6, 034001. https://doi.org/10.1088/1748-9326/6/3/034001.
Mlawer, Eli, J., Taubman, S.J., Brown, P.D., Iacono, M.J., Clough, S.A., 1997. Radiative transfer for inhomogeneous atmospheres: RRTM, a validated correlated-k model for the longwave. J. Geophys. Res. 102, 16663–16682. https://doi.org/10.1029/97JD00237.
Mohan, M., Gupta, A., Bhati, S., 2014. A modifed approach to analyze thermal comfort classifcation. Atmos. Clim. Sci. 4, 13. https://doi.org/10.4236/acs.2014.41002.
Monin, A.S., Obukhov, A.M., 1954. Basic Laws of turbulent mixing in the surface layer of the atmosphere. Contrib. Geophys. Inst. Acad. Sci. USSR 24, 163–187.
Morini, E., Touchaei, A.G., Rossi, F., Cotana, F., Akbari, H., 2017. Evaluation of albedo enhancement to mitigate impacts of urban heat island in Rome (Italy) using WRF meteorological model. Urban Clim. 24, 551–566. https://doi.org/10.1016/j.uclim.2017.08.001.
Mussetti, G., Brunner, D., Henne, S., Allegrini, J., Krayenhoff, E.S., Schubert, S., Feigenwinter, C., Vogt, R., Wicki, A., Carmeliet, J., 2020. COSMO-BEP-tree v1.0: a coupled urban climate model with explicit representation of street trees. Geosci. Model Dev. 13, 1685–1710. https://doi.org/10.5194/gmd-13-1685-2020.
Nowak, D.J., Hirabayashi, S., Bodine, A., Greenfield, E., 2014. Tree and forest effects on air quality and human health in the United States. Environ. Pollut. 193, 119–129. https://doi.org/10.1016/j.envpol.2014.05.028.
Owinoh, A.Z., Hunt, J.C., Orr, A., Clark, P., Klein, R., Fernando, H.J.S., Nieuwstadt, F.T., 2005. Effect of changing surface heat flux on atmospheric boundary-layer flow over flat terrain. Bound.-Layer Meteor. 116, 331–361.
Patel, P., Karmakar, S., Ghosh, S., Niyogi, Dev, 2020. Improved simulation of very heavy rainfall events by incorporating WUDAPT urban land use/land cover in WRF. Urban Clim. 32, 100616. https://doi.org/10.1016/j.uclim.2020.100616.
Poulos, G.S., Blumen, W., Fritts, D.C., Lundquist, J.K., Sun, J.L., Burns, S.P., Nappo, C., Banta, R., Newsom, R., Cuxart, J., Terradellas, E., Balsley, B., Jensen, M., 2002. CASES-99: a comprehensive investigation of the stable nocturnal boundary layer. Bull. Amer. Meteor. Soc. 83, 555–581. https://doi.org/10.1175/1520-0477(2002)083,0555:CACIOT.2.3.CO;2.
Qian, Y., Chakraborty, T.C., Li, J., Li, D., He, C., Sarangi, C., Chen, F., Yang, X., Leung, L.R., 2022. Urbanization impact on regional climate and extreme weather: current understanding, uncertainties, and future research directions. Adv. Atmos. Sci. 39, 819–860. https://doi.org/10.1007/s00376-021-1371-9.
Ribeiro, I., Martilli, A., Falls, M., Zonato, A., Villaba, G., 2020. Highly resolved WRF-BEP/BEM simulations over Barcelona urban area with LCZ. Atmos. Res. 248, 105220. https://doi.org/10.1016/j.atmosres.2020.105220.
Ricard, S., Badia, A., Ventura, S., Gilabert, J., Martilli, A., Villalba, G., 2021. Sensitivity study of PBL schemes and soil initialization using the WRF-BEP-BEM model over a Mediterranean coastal city. Urban Clim. 39, 100982. https://doi.org/10.1016/j.uclim.2021.100982.
Rothfusz, L.P., 1990. The heat index equation (or, more than you ever wanted to know about heat index). Tech. Attachment, SR/SSD 90-23, U.S. National Weather Service, Southern Regional Headquarters, Forth Worth, TX. https://www.weather.gov/media/fc/ta_htindx.PDF.
Salamanca, F., Martilli, A., 2010. A new building energy model coupled with an urban canopy parameterization for urban climate simulations—part II. Validation with one dimention off-line simulations. Theor. Appl. Climatol. 99, 345. https://doi.org/10.1007/s00704-009-0143-8.
Salamanca, F., Krpo, A., Martilli, A., Clappier, A., 2010. A new building energy model coupled with an urban canopy parameterization for urban climate simulations - part I. Formulation, verification, and sensitivity analysis of the model. Theor. Appl. Climatol. 99 (3–4), 331–344. https://doi.org/10.1007/s00704-009-0142-9.
Salamanca, F., Martilli, A., Tewari, M., Chen, F., 2012. A study of the urban boundary layer using different urban parameterizations and high-resolution urban canopy parameters with WRF. J. Appl. Meteorol. Climatol. 50, 1107–1128. https://doi.org/10.1175/2010JAMC2538.1.
Salamanca, F., Tonse, S., Menon, S., Garg, V., Singh, K.P., Naja, M., Fischer, M.L., 2012a. Top-of-atmosphere radiative cooling with white roofs: experimental verification and model-based evaluation. Environ. Res. Lett. 7, 044007. https://doi.org/10.1088/1748-9326/7/4/044007.
Salamanca, F., Georgescu, M., Mahalov, A., Moustaoui, M., Martilli, A., 2016. Citywide impacts of cool roof and rooftop solar photovoltaic deployment on near-surface air temperature and cooling energy demand. Bound.-Layer Meteorol. 161, 203–221. https://doi.org/10.1007/s10546-016-0160-y.
Santamouris, M., 2014. Cooling the cities—A review of reflective and green roof mitigation technologies to fight heat island and improve comfort in urban environments. Sol. Energy 103, 682–703. https://doi.org/10.1016/j.solener.2012.07.003.
Santiago, J.L., Martilli, A., 2010. A dynamic urban canopy parameterization for mesoscale models based on computational fluid dynamics reynoldsaveraged Navier–Stokes microscale simulations. Bound.-Layer Meteorol. 137 (3), 417–439. https://doi.org/10.1007/s10546-010-9538-4.
Scherba, A., Sailor, D.J., Rosenstiel, T.N., Wamser, C.C., 2011. Modeling impacts of roof reflectivity, integrated photovoltaic panels and green roof systems on sensible heat flux into the urban environment. Build. Environ. 46 (12), 2542–2551. https://doi.org/10.1016/j.buildenv.2011.06.012.
Sharma, A., Conry, P., Fernando, H.J.S., Alan, F.H., Hellmann, J.J., Chen, F., 2016. Green and cool roofs to mitigate urban heat island effects in the Chicago metropolitan area: evaluation with a regional climate model. Environ. Res. Lett. 11 (6), 064004. https://doi.org/10.1088/1748-9326/11/6/064004.
Skamarock, W.C., Klemp, J.B., Dudhia, J., Gill, D.O., Liu, Z., Berner, J., Wang, W., Powers, J.G., Duda, M.G., Barker, D.M., Huang, X.-Y., 2021. A Description of the Advanced Research WRF Version 4.3, (No. NCAR/TN-556+STR). https://doi.org/10.5065/1dfh-6p97.
Steadman, R.G., 1979. The assessment of sultriness. Part I: a temperature-humidity index based on human physiology and clothing science. J. Appl. Meteor. 18, 861–873. https://doi.org/10.1175/1520-0450(1979)018<0861:TAOSPI>2.0.CO;2.
Stewart, I.D., Oke, T.R., 2012. Local climate zones for urban temperature studies. Bull. Am. Meteorol. Soc. 93 (12), 1879–1900. https://doi.org/10.1175/BAMS-D-11-00019.1.
Sun, T., Bou-Zeid, E., Wang, Z.-H., Zerba, E., Ni, G.-H., 2013. Hydrometeorological determinants of green roof performance via a vertically-resolved model for heat and water transport. Build. Environ. 60, 211–224. https://doi.org/10.1016/j.buildenv.2012.10.018.
Sun, T., Bou-Zeid, E., Ni, G.-H., 2014. To irrigate or not to irrigate: analysis of green roof performance via a vertically-resolved hygrothermal model. Build. Environ. 73, 127–137. https://doi.org/10.1016/j.buildenv.2013.12.004.
Sun, T., Grimmond, C.S.B., Ni, G.-H., 2016. How do green roofs mitigate urban thermal stress under heat waves? J. Geo. Res: Atmos. 121, 5320–5335. https://doi.org/10.1002/2016JD024873.
Synnefa, A., Dandou, A., Santamouris, M., Tombrou, M., Soulakellis, N., 2008. On the use of cool materials as a heat island mitigation strategy. J. Appl. Meteorol. Clim. 47, 2846–2856. https://doi.org/10.1175/2008JAMC1830.1.
Taha, H., 2013. The potential for air-temperature impact from large-scale deployment of solar photovoltaic arrays in urban areas. Sol. Energy 91, 358–367. https://doi.org/10.1016/j.solener.2012.09.014.
Tan, H., Ray, P., Tewari, M., Brownlee, J., Ravindran, A., 2019. Response of near-surface meteorological conditions to ddvection under impact of the green roof. Atmosphere 10, 759. https://doi.org/10.3390/atmos10120759.
Wang, X., Li, H., Sodoudi, S., 2022. The effectiveness of cool and green roofs in mitigating urban heat island and improving human thermal comfort. Build. Environ. 217, 109082. https://doi.org/10.1016/j.buildenv.2022.109082.
Wong, N.H., Chen, Y., 2005. Study of green areas and urban heat island in a tropical city. Habit. Int. 29 (3), 547–558. https://doi.org/10.1016/j.habitatint.2004.04.008.
Yang, J., Yu, Q., Gong, P., 2008. Quantifying air pollution removal by green roofs in Chicago. Atmos. Environ. 42, 7266–7273. https://doi.org/10.1016/j.atmosenv.2008.07.003.
Yang, J.C., Wang, Z.-H., Georgescu, M., Chen, F., Tewari, M., 2016. Assessing the impact of enhanced hydrological processes on urban hydrometeorology with application to two cities in contrasting climates. J. Hydrometeorol. 17 (4), 1031–1047. https://doi.org/10.1175/JHM-D-15-0112.1.
Yip, F.Y., Flanders, W.D., Wolkin, A., Engelthaler, D., Humble, W., Neri, A., Lewis, L., Backer, L., Rubin, C., 2008. The impact of excess heat events in Maricopa County, Arizona: 2000–2005. Int. J. Biometeorol. 52, 765–772. https://doi.org/10.1007/s00484-008-0169-0.
Zhang, J.C., Li, Y., Tao, W., Liu, J.F., Levinson, R., Mohegh, A., Ban-Weiss, G., 2019. Investigating the urban air quality effects of cool walls and cool roofs in southern California. Environ. Sci. Technol. 53 (13), 7532–7542. https://doi.org/10.1021/acs.est.9b00626.
Zhang, N., Chen, Y., Luo, Ling, Wang, Y.W., 2017. Effectiveness of different urban Heat Island mitigation methods and their regional impacts. J. Hydro. 18 (11), 2991–3012. https://doi.org/10.1175/JHM-D-17-0049.1.
Zilitinkevich, S.S., Hunt, J.C.R., Esau, I.N., Grachev, A.A., Lalas, D.P., Akylas, E., Joffre, S.M., 2006. The influence of largeconvective eddies on the surface-layer turbulence. Q. J. R. MeteorolSoc. 132, 1426–1456.
Zonato, A., Martilli, A., Sabatino, S.Di., Zardi, D., Giovannini, L., 2020. Evaluating the performance of a novel WUDAPT averaging technique to define urban morphology with mesoscale models. Urban Clim. 31, 100584. https://doi.org/10.1016/j.uclim.2020.100584.
Zonato, A., Martilli, A., Gutierrez, E., Chen, F., He, C., Barlage, M., Zardi, D., Giovannini, L., 2021. Exploring the effects of rooftop mitigation strategies on urban temperature and energy consumption. J. Geophys. Res. Atmos. 126, e2021JD035002. https://doi.org/10.1029/2021JD035002.